Catalytic functionalization of hexagonal boron nitride for oxidation and epoxidation reactions by molecular oxygen

Min Gao[1], Ben Wang[2], Takao Tsuneda[3,4], Andrey Lyalin[5,6], and Tetsuya Taketsugu[3,5*]*

[1] Institute for Catalysis, Hokkaido University, Sapporo 001-0021, Japan

[2] Graduate School of Chemical Sciences and Engineering, Hokkaido University, Sapporo 060-0810, Japan

[3] Department of Chemistry, Faculty of Science, Hokkaido University, Sapporo 060-0810, Japan

[4] Graduate School of Science Technology and Innovation, Kobe University, Nada-ku, Kobe, Hyogo 657-8501, Japan

[5] Institute for Chemical Reaction Design and Discovery (WPI-ICReDD), Hokkaido University, Sapporo 001-0021, Japan

[6] Center for Green Research on Energy and Environmental Materials (GREEN), National Institute for Materials Science, Namiki 1-1, Tsukuba 305-0044, Japan

ABSTRACT

The mechanism of catalytic oxidation of carbon monoxide and epoxidation of ethylene by molecular oxygen adsorbed on the carbon-doped hexagonal boron nitride (h-BN) is investigated theoretically. The energy profiles and the dependence of the activation barriers on the distance between the doped carbon atom are analyzed. It is shown that the considered oxidation and epoxidation reactions can occur not only on the B atom sites in the close vicinity to the C dopant but also at relatively large distances from the C dopant. Therefore, C_B/h-BN possesses many active sites and it is possible to achieve a wide activation area (~5.0 Å from the doped C) of the catalyst at the small concentration of C. The results of calculations demonstrate that the reaction intermediates along these reaction pathways are slightly destabilized with an increase in the distance from the doped C atom; however, the reaction barriers remain mainly intact. Therefore, C doping of h-BN is a highly promising way for catalytic functionalization of the inert h-BN based materials for oxidation and epoxidation reactions by molecular oxygen.

KEYWORDS: carbon monoxide oxidation, ethylene epoxidation, carbon-doped hexagonal boron nitride catalyst, distance effects

I. Introduction

Heterogeneous catalysts for activation and dissociation of molecular oxygen play an important role in a wide range of industrial applications, such as combustion, selective oxidation, electrochemical reactions in fuel cells, etc.[1,2] Considerable efforts have been made for the design of effective catalysts for chemical reactions with molecular oxygen. Most of the industrially used catalysts for these reactions are based on platinum-group metals (PGMs) which can considerably promote the oxidation processes.[3,4] Despite the high efficiency of PGMs catalysts, their low abundance, and the high market value strongly limit their industrial applications.[4] Therefore, the development of new effective PGMs free and low-cost catalysts for molecular oxygen activation is highly demanding.[5,6]

Two-dimensional (2D) metal-free materials such as graphene can be of potential interest for catalytic applications because of the wide surface area and valuable physical and chemical properties. However, pure graphene is inactive due to its delocalized uniform charge distribution.[7] To activate its catalytic performance, various dopants or vacancy defects should be incorporated into the surface. Theoretical and experimental studies have suggested that the inclusion of single transition metal or non-metal heteroatoms (N, P, S, B etc.) into graphene enables the electronic structure and electron distribution to achieve high catalytic activity.[8-10] Thus, it has been established that graphene doped with N and B atoms becomes an active catalyst for reactions of aerobic oxidation.[11]

Hexagonal boron nitride (h-BN) monolayer is a 2D material with a geometry structure similar to graphene, but contrary to graphene possessing insulating properties with a wide bandgap and high thermal stability.[12] For many years, h-BN has been considered to be an inactive catalyst. However, recently it was demonstrated that h-BN can be functionalized by atomic doping, defect

formation and metal supports to reveal its unusual catalytic properties.[12-23] That is, the induced defect states in the forbidden zone of h-BN promote the interaction and activation of the adsorbed O_2 with the catalyst.[12] Recently, we have shown that the h-BN nanosheets deposited on the Au(111) support possess superior electrocatalytic activity for oxygen reduction reaction (ORR)[16,24] and hydrogen evolution reaction (HER).[19] In the case of the HER, we have achieved the catalytic activity of BN/Au similar to that known for Pt surface, which is accepted as one of the best catalysts. Though these BN-based materials considered above enhance the potential for the development of efficient metal-free catalysts, there are still serious limitations: the catalytically active sites are restricted to their dopant atoms or the small areas in the close vicinity of the dopant hetero-atoms.

For activation of the adsorbed O_2, catalysts should meet, at least, two requirements: (i) the adsorption energy should be neither too low in order to keep the activated O_2 bonded to the surface, nor too high in order to let reaction products depart from the surface after the reaction; (ii) the surface area where O_2 can be adsorbed in the activated form should be large enough to increase the efficiency of the O_2 involved reaction. So far, PGMs based catalysts have been accepted as suitable and effective catalysts for achieving these two requirements in various reactions.[25,26] The studies on 2D catalysts possessing wide areas with active sites which are comparable with the surface area of the whole 2D sheets have been limited. The predictive theoretical design of novel catalysts can overcome this limitation.

Recently, we found that substitutional doping of C atom into a position of B atom in 2D h-BN sheet (C_B@h-BN) generates *n*-type semiconducting material with noticeable catalytic activity for the O_2 activation over the large area extended far from the doped C impurity.[27] Although pristine h-BN monolayer is inert for O_2 adsorption and activation, the C-doped C_B@h-BN sheet

can trap and activate O_2 even far from the C defect. It was found that the catalytically active area in C_B@h-BN highly depends on the energy gap between the highest occupied defect level of the doped C atom and the bottom of the conduction band of the h-BN monolayer. In particular, in the case of O_2 activation, the defect states should be delocalized and position themselves near the bottom of the conduction band to activate the atoms of the h-BN monolayer, which are far from C dopant. Note that it has been reported that usual DFT functionals tend to give wide activation area by the erroneous electron delocalization due to the lack of long-range exchange effects. Janesko suggested that in a C-doped H-edged BN nanoribbon model, the long-range exchange effects by the long-range correction for exchange functionals narrow the O_2 activation area.[28] However, it has also been shown that even with the use of the long-range corrected functionals, the large area within the distances of ~5.0 Å from the doped C atom remains active. It is also possible that the effect induced by C atoms can be further enhanced by the increase in the concentration of doped C atoms. Therefore, carbon doping can trigger functionalization of the large surface area for oxygen adsorption and activation in comparison with other hetero-atoms dopants.

In this study, we aim to investigate the dependence of the activation barriers for typical oxidation reactions as a function of the distance between the doped C atom and the reaction sites. The reactions of CO oxidation and C_2H_4 epoxidation by molecular oxygen were chosen as model reactions due to their industrial and fundamental importance. By analyzing the energy profiles and the dependence of the activation barriers on the distance between reaction sites and the doped carbon atom, it is demonstrated that the considered oxidation and epoxidation reactions can occur not only on the sites directly connected to the C dopant but also at the relatively long distances from the dopant. Therefore, the C-doped h-BN monolayer can serve as a good catalyst for oxidation reactions by molecular oxygen.

II. Computational Details

Calculations are carried out using density functional theory (DFT) with the Wu-Cohen (WC) generalized-gradient-approximation (GGA) exchange-correlation functional[29] as implemented in the PWSCF (Plane-Wave Self-Consistent Field) program of Quantum ESPRESSO package.[30] It has been reported that the WC functional correctly reproduces the lattice constants, crystal structures, and surface energies of solids with layered structures such as graphite or h-BN with the weal interaction between layers.[14] A plane-wave basis set is used with Troullier-Martins norm-conserving pseudopotentials. All the calculations are performed using the spin-polarized electronic structures and periodic boundary conditions for all systems. The energy cutoff of 80 Ry is chosen to make sure the convergence in total energies and forces. The lattice of bulk h-BN was optimized using the Monkhorst-Pack 10×10×4 k-point mesh for Brillouin zone sampling. The calculated lattice parameters a = b = 2.504 Å, and c = 6.656 Å are in excellent agreement with the experimental ones:[31] a = b = 2.524 ± 0.020 Å and c = 6.684 ± 0.020 Å. A climbing image nudged elastic band (CI-NEB) method is adopted to search transition states and minimum energy pathways.[32] The atoms in molecules method (AIM) is used for the charge analysis.[33] The electron density difference is illustrated by VESTA.[34] The h-BN surface is represented by the one-layer slab containing 6×6 unit cells. The periodically replicated slabs are separated by the vacuum region of 15 Å in the (001) direction. Only the Γpoint is used for sampling the Brillouin zone due to the large size of the supercell. The adsorption energies were calculated by the equation, $E_{ad} = E_{tot} - E_{C@h\text{-}BN} - E_{O2} - E_{mol}$, where E_{tot}, $E_{C@h\text{-}BN}$, E_{O2}, E_{mol} indicate the electronic energy of the whole system, the C-doped monolayer C@h-BN, the isolated oxygen molecule, and the reactant CO/C_2H_4 molecules, respectively. The rate constant k was calculated using Eyring equation, $k = k_B T/h \exp(-\Delta G/RT)$, with transmission coefficient = 1, where k_B is Boltzmann constant, h is Planck

constant; ΔG is a change in Gibbs free energy, R is the universal gas constant and T is temperature. In the present work, we consider chemical transformations between the species adsorbed on the surface. Therefore, translational degrees of freedom, giving the major contribution to the entropic term of free energy are frozen. In this case, we can approximate ΔG by the value of activation energy E_a without considerable loss in accuracy.

III. Results and Discussions

Adsorption sites of O_2, CO, and C_2H_4 molecules on the C-doped h-BN surface

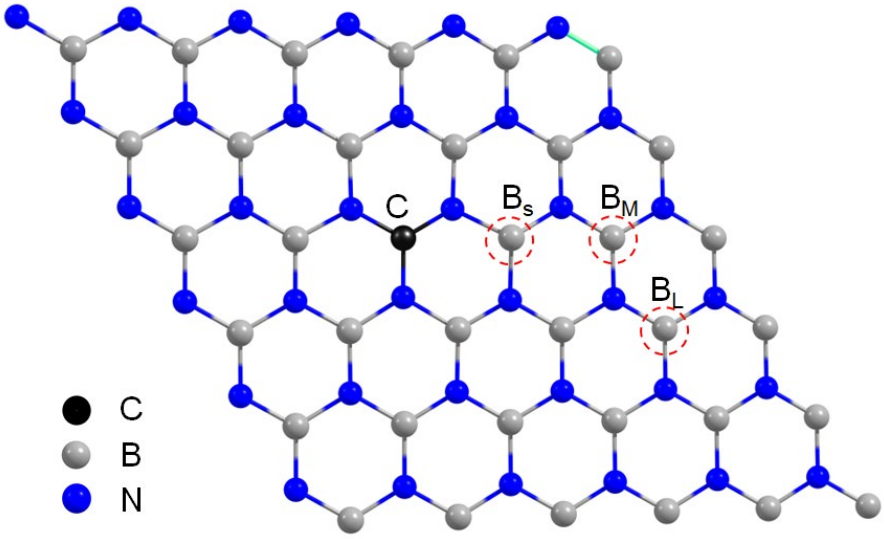

Figure 1. Computational model for the C-doped h-BN monolayer. The B sites in red circle was chosen as active sites for oxygen molecule. The C, B, N atoms are shown in black, gray and blue, respectively.

Let us consider the adsorption of O_2, CO, and C_2H_4 molecules on the h-BN monolayer doped with the C atom into B position, C_B@h-BN. To obtain the most stable structures of CO and C_2H_4 molecules on the C_B@h-BN, a large number of initial configurations were considered at multiple possible reaction sites, followed by the full optimization of the total system. A similar approach has been successfully used in our previous work.[18] As O_2 molecule only adsorbs on the B sites,[18] we considered three different adsorption sites, B_S, B_M, B_L (**Figure 1**) with the distances from the C atom of 2.49, 4.98, and 6.62 Å, respectively. We would like to note that the B_L site is expected to be less active because, as mentioned in Sec. I, the activation area should be limited to

the distance of ~5 Å from the doped C atom due to the long-range exchange effects.[28] In our previous study,[18] we have performed a theoretical analysis of a single atom substitutional doping of C to B and N positions in h-BN and found out that such doping does not affect the planar geometry structure of the h-BN sheet. However, C doping considerably affects the electronic structure of the h-BN monolayer, resulting in the appearance of defect levels in the forbidden zone. It was found that the occupied 2*p* state of the doped C atom at the bottom of the conduction band of h-BN considerably affects the chemical properties of the doped sheet, promoting O_2 adsorption and activation in the surface area extending from the doped C atom.

Figure 2 shows the most stable optimized structures of O_2, CO, and C_2H_4 molecules adsorbed in the vicinity of C_B impurity in the h-BN monolayer. CO molecule weakly adsorbs on top of the C site with the adsorption energy of -0.19 eV (-4.4 kcal/mol), while it has a very small interaction with the B site atoms with the adsorption energy of -0.08 eV (-1.8 kcal/mol). The C-C bond length between CO and the C_B@h-BN is 2.44 Å, and the CO distance hardly changes from that of the isolated CO molecule, indicating no electron transfer between CO and the surface. Similar to the CO adsorption, C_2H_4 weakly adsorbs the doped C atom site of the C_B@h-BN surface with the adsorption energy of -0.15 eV (-3.4 kcal/mol), while no interaction was found with the other sites. In a contrast to the cases of CO and C_2H_4 adsorption, the O_2 molecule adsorbs not only at the doped C site but also at the B sites located relatively far from the doped C atom. A detailed investigation on the adsorption of O_2 molecule on C_B@h-BN has been reported in our previous study:[18] O_2 molecule can bind on top of B atom (top site) or bridge two nearest B atoms (bridge site) on C_B@h-BN. The adsorption energies of the O_2 molecule on the top of B_S, B_M, and B_L sites are -1.46, -0.98, and -0.85 eV (i.e., -34, -23, and -20 kcal/mol), respectively. The adsorption of O_2 molecule at bridge sites is slightly weaker than the top ones and is accompanied by structural

deformation of C_B@h-BN. It has been shown that the adsorption energy of the O_2 molecule on C_B@h-BN highly depends on the distance between the adsorption sites and the doped C atom site. As increasing this distance, the absolute value of the O_2 adsorption energy gradually decreases. Single point calculations using a short-range hybrid HSE06 functional were carried out to confirm the distance dependence on the adsorption energies of O_2 molecule. As a result, we found that the HSE06 functional gives slightly smaller adsorption energies (-1.37 at B_S, -0.83 at B_M, and -0.66 eV B_L sites) if compared to those of the *Wu-Cohen* functional due to the lack of the long-range correction. Adsorption of the second O_2 molecule was also considered to clarify the effect of the doped carbon on the catalytic activity of h-BN surface. No interaction was found between the second O_2 and O_2/C_B@h-BN due to the considerable electron transfer between C_B@h-BN and the first O_2. Note that these adsorption energies are much larger than those of the CO and C_2H_4 molecules. After O_2 adsorption, two main pathways have been proposed for the oxidation reaction:[14] In one pathway, the preliminary dissociation of the adsorbed O_2 molecule, which leads to the oxidation of the reactant molecule using the dissociated O atoms. In another pathway, the reactant molecule directly interacts with the activated O_2 molecule. In this study, we take into consideration both of these pathways.

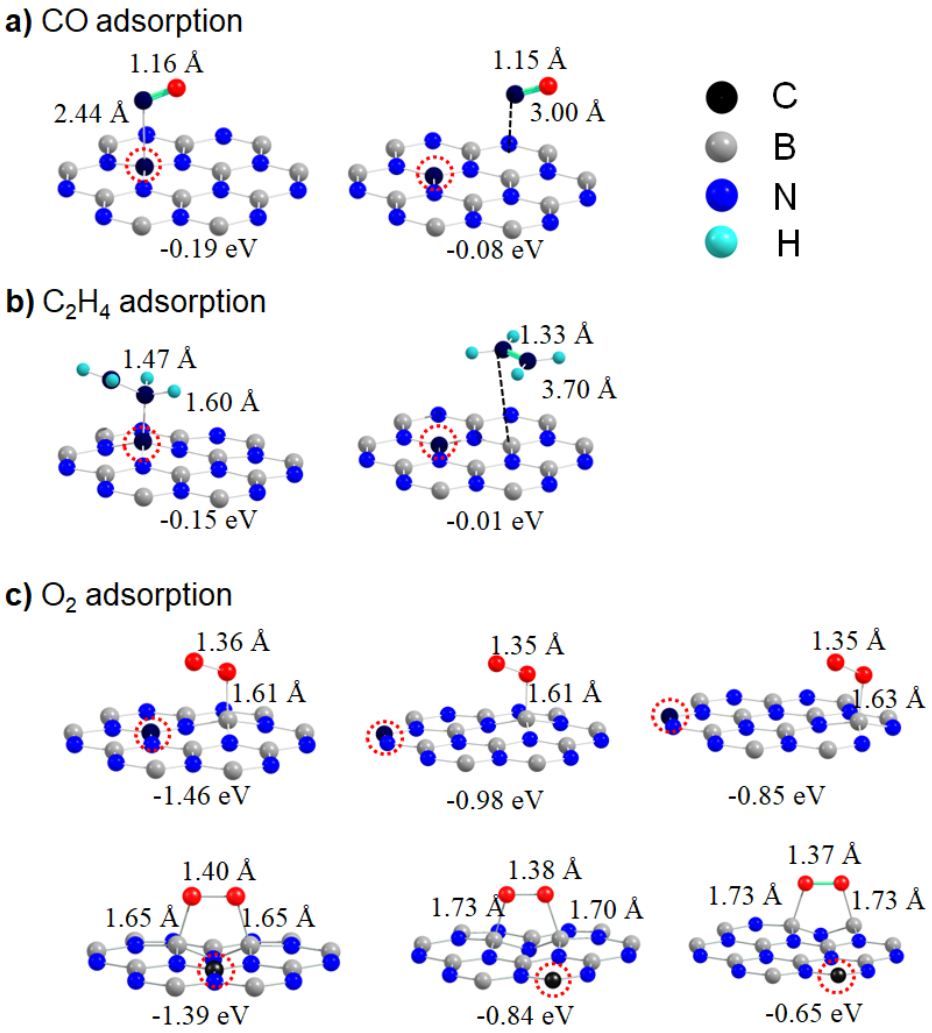

Figure 2. Optimized structures of CO, C_2H_4 and O_2 molecules adsorbed on the C_B@h-BN monolayer. The corresponding adsorption energies are shown below each structure. Only part of the C_B@h-BN monolayer is shown. The interatomic distances are given in Å. The dashed circle in red indicates the position of doped C atom.

CO oxidation reaction mechanism on the C-doped h-BN

Next, we focus on the possible reaction pathways for CO and C_2H_4 oxidation reactions catalyzed by C_B@h-BN. There are many studies devoted to the detailed investigation of the different aspects of CO oxidation reaction.[35-43] The mechanism of CO oxidation is generally classified into two types: Langmuir-Hinshelwood (LH) mechanism, in which CO and O_2 co-adsorb on the catalytic surface and react with each other, and Eley-Rideal (ER) mechanism, in which gas CO molecules react with the adsorbed O_2 molecule directly. In our previous study,[14] we found the CO oxidation on h-BN surface proceeds with the support of gold cluster in either the ER mechanism or a self-promotion mechanism following the bimolecular LH mechanism. As the O_2 adsorption on C_B@h-BN is much stronger than the CO adsorption, we focus on the CO oxidation reaction mechanism by an activated O_2 molecule on C_B@h-BN. After the O_2 adsorption and activation, there are two possible pathways for the catalytic oxidation on C_B@h-BN: (i) CO molecule reacts with atomic oxygen, which is generated by the preliminary dissociation of adsorbed O_2; (ii) CO molecule attacks the activated adsorbed O_2.

It has been found that the barrier of O_2 dissociation on the C_B@h-BN surface is about 1.83 eV which is too high to break O−O bond without additional reactions. Therefore, CO oxidation is supposed to follow the second pathway, i.e., the direct reaction of CO with O_2 activated on the C_B@h-BN surface.

The results of calculations demonstrate that O_2 adsorbs on top of the B_S site (B atom nearest to the C impurity) as well as bridges two B_S sites with the adsorption energies of -1.47 eV and -1.39 eV, respectively. We have found that adsorbed O_2 molecule can react with the coming CO in three possible scenarios: (1) a carbonate-like (CO_3) intermediate is formed by the insertion of CO molecule to the O-O bond of O_2 at the bridge site; (2) a peroxide-like OCOO intermediate is

produced by attaching the adsorbed O_2 with CO at the B sites of the surface; and (3) the first CO_2 molecule is formed by the direct reaction of gas CO and adsorbing O_2 molecules.

According to the results of our calculations, the formation of the carbonate-like intermediate from the reaction of CO and adsorbed O_2 along the pathway (1) is very slow due to the high activation barrier of 1.25 eV (28.8 kcal/mol). The high barrier mainly comes from the O-O bond breaking during the CO insertion. On the other hand, the peroxide-like OCOO intermediate INT_2 in the pathway (2) is exothermically formed through $TS_{1\text{-}2}$ with a considerably lower activation barrier, 0.24 eV (5.5 kcal/mol), as shown in **Figure 3**. The lowering of the activation barrier can be a result of a strong interaction between CO and O_2 molecules.[44] The co-adsorption of CO molecule elongates the O-O bond of O_2 molecule to 1.49 Å. Furthermore, the OCOO intermediate is easily decomposed into CO_2 molecule through $TS_{2\text{-}3}$ in Figure 3 with the low activation barrier of 0.25 eV (5.7 kcal/mol), while the residual O atom strongly adsorbs the surface (INT_3 in Figure 3) with the adsorption energy of -4.37 eV (-100.8 kcal/mol). The energy pathway through the OCOO intermediate is called the "*self-promoting pathway*", because the co-adsorption of CO facilitates the O-O bond breaking. For pathway (3), the adsorbed O_2 reacts with gas CO molecule to form the first CO_2 through TS'_1 with a relatively low activation energy, 0.29 eV (6.7 kcal/mol), while the residual O atom forms INT_3 adsorption structure on the C_B@h-BN surface. This pathway is called the "*direct pathway*" because the CO molecule directly reacts with the absorbed O_2. The low activation energies in the pathways (2) and (3) suggest that the first CO_2 molecule is formed in the self-promoting and direct pathways on the C_B@h-BN surface.

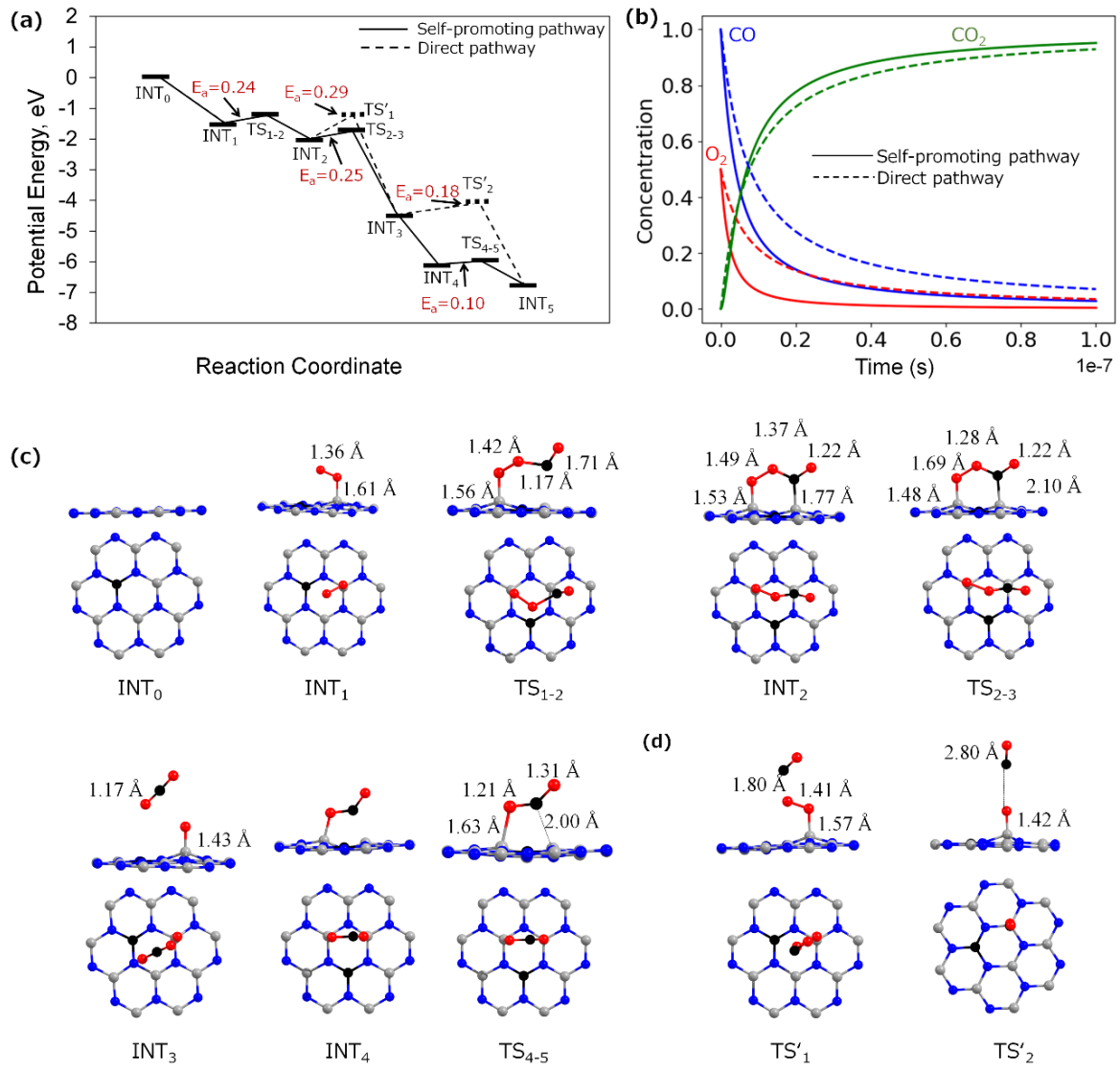

Figure 3. (a) Energy profiles of CO oxidation at B_S site of C_B@BN monolayer via the self-promoting pathway (solid line) and the direct pathway (dashed line). (b) microkinetic simulation for self-promoting pathway and the direct pathway at 300 K. The corresponding geometries for energy profiles are also shown in (c) and (d), respectively. The overlapped geometries were only shown in (c). Only part of the h-BN monolayer is shown.

Similar to the formation of the first CO_2 molecule, the formation of the second CO_2 molecule from INT_3 (see Figure 3) has two possible pathways: (i) the residual O atom in INT_3 reacts with CO to produce OCO at the B sites of the surface; and (ii) the second CO_2 molecule is formed by the direct reaction of gas CO molecule with the residual O atom in INT_3. The energy barriers for these two possible paths are similar, 0.18 eV (4.2 kcal/mol) and 0.10 eV (2.3 kcal/mol) and therefore these paths are competitive. As INT_3 is a quite stable structure giving the small activation barriers for the second CO_2 formation, this result indicates that the first CO_2 formation is the rate-determining step. Microkinetic simulations[45] were performed to compare the self-promoting pathway and the direct pathway as shown in Figure 3(b). The following steps were considered for (a) the self-promoting pathways: O_2* + CO (g) ↔ O_2-CO*; O_2-CO* + CO (g) ↔ CO_2 (g) + OCO*; OCO* ↔ CO_2 (g); (b) the direct pathways, O_2* + CO (g) ↔ CO_2 (g) + O*; O* + CO (g) ↔ CO_2 (g), where the * indicates C_B@h-BN surface and g indicates gas phase. The initial concentration of CO/O_2 was set to 2:1 at 300 K. It was shown that the consumption rate of CO and O_2 is larger for the self-promoting pathway, though CO_2 can be generated through both the self-promoting and direct pathways as the reaction rate is fast enough. The amount of the generated CO_2 is similar at the initial stage of these two pathways, while it becomes slightly higher for the self-promoting pathway if compared with the direct one as the reaction proceeds further.

In summary, the results of calculations suggest that CO oxidation on C_B@h-BN surface proceeds in the following steps (here asterisk * denotes C_B@h-BN surface):

(1) $O_2 + * \rightarrow O_2*$,

(2) $CO + O_2* \rightarrow OCOO*$ or $CO + O_2* \rightarrow CO_2 + O*$ (rate-determining step),

(3) $OCOO* \rightarrow CO_2 + O*$,

(4) $CO + O^* \rightarrow OCO^*$ or $CO + O^* \rightarrow CO_2 + *$,

(5) $OCO^* \rightarrow CO_2 + *$.

Distance effects of CO oxidation on the C-doped h-BN surface

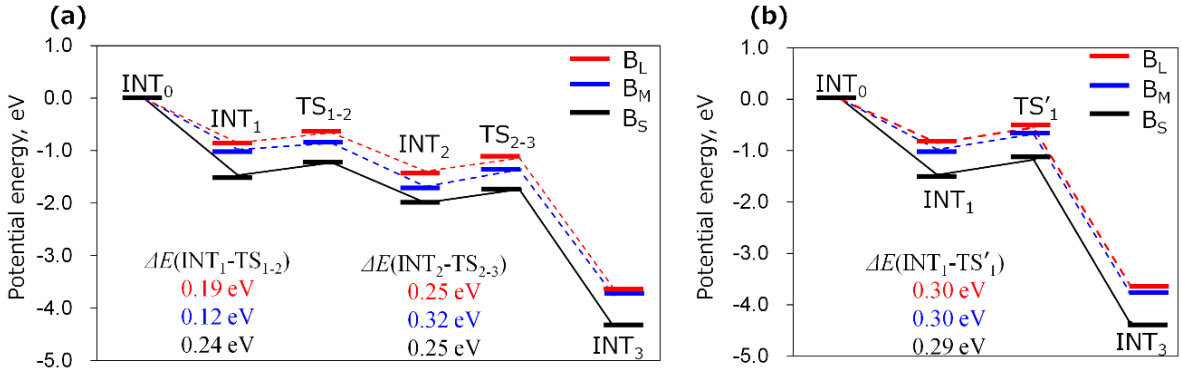

Figure 4. The distance effect on the reaction pathways for catalytic CO oxidation in the case of (a) the self-promoting pathway; (b) the direct pathway a. The black, blue and red lines indicate reaction pathways calculated at the B_S, B_M, and B_L sites, respectively.

We also explore how the energetics of the rate-determining step of the first CO_2 formation depends on the distance from the doped C atom on the C_B@h-BN surface. As was mentioned above, we have considered three different reaction sites B_S, B_M, and B_L with distances from the doped C atom of 2.49, 4.98, and 6.62 Å, respectively. **Figures 4a and 4b** demonstrate the energy profiles for CO oxidation calculated at the different reaction sites for the self-promoting and the direct pathways, respectively. As it is seen from Figure 4, the energy profiles are slightly shifting up with an increase in the distance between the reaction site and the doped C atom. The energies of the intermediates and transition states are increasing by ~0.53 eV (12 kcal/mol) from B_S site to B_M site and by ~0.66 eV (15 kcal/mol) from B_S site to B_L, while the energy barriers for transitions from INT_1 to INT_2 and INT_2 to INT_3 are hardly affected by the distance effects. In the case of the self-promoting pathway, the activation energies of the CO_2 formation are calculated as 0.25, 0.32, and 0.25 eV for the B_S, B_M, and B_L sites, respectively. Although the activation energy calculated

for the reaction at the B_M site is a little higher, it is low enough to be overcome at room temperature. **Table 1** presents the dependence of the calculated rate constants on temperature. For self-promoting pathways, the predicted rate constants are evaluated as 10^8~10^{10} s^{-1} for $k_{INT1\text{-}TS1\text{-}2}$ and 10^7~10^8 s^{-1} for $k_{INT2\text{-}TS2\text{-}3}$ at 300K, indicating all the B_S, B_M and B_L sites are active. The rate constant, $k_{INT1\text{-}TS1\text{-}2}$ at the B_M site ($k_{INT1\text{-}TS1\text{-}2}$@$B_M$) is 100 and 15 times larger than those at B_S ($k_{INT1\text{-}TS1\text{-}2}$@$B_S$) and B_L ($k_{INT1\text{-}TS1\text{-}2}$@$B_L$) sites, respectively. At 600K, the rate constants ratio of $k_{INT1\text{-}TS1\text{-}2}$@$B_M$/ $k_{INT1\text{-}TS1\text{-}2}$@$B_S$, and $k_{INT1\text{-}TS1\text{-}2}$@$B_M$/ $k_{INT1\text{-}TS1\text{-}2}$@$B_L$ decrease 10, 3.8 times, respectively. A similar trend was also found for $k_{INT2\text{-}TS2\text{-}3}$. This indicates that the activities of the sites significantly depend on the temperature in the self-promoting pathways, and the effect of distance from the active site to C dopant on the reaction activity becomes smaller. The rate constants ($k_{INT1\text{-}TS1'}$) of the direct pathways are slightly smaller than those of the self-promoting pathways. B_S, B_M, and B_L sites possess similar reaction rates independent of temperature for the direct pathways in contrast to those for the self-promoting pathways. Therefore, this result indicates that the activities of the B_S, B_M and B_L sites have very different temperature-dependence for the self-promoting pathways, though they give similar temperature-dependence for the direct pathways: the activation energies are 0.29, 0.30, and 0.30 eV for the B_S, B_M and B_L sites, respectively.

Table 1. The rate constants at different temperatures for CO oxidation pathways in Figure 4.

	$k_{(INT1\text{-}TS1\text{-}2)}$, s^{-1}			$k_{(INT2\text{-}TS2\text{-}3)}$, s^{-1}			$k_{(INT1\text{-}TS'1)}$, s^{-1}		
	B_S	B_M	B_L	B_S	B_M	B_L	B_S	B_M	B_L
300 K	6.1×10^{8}	6.4×10^{10}	4.3×10^{9}	5.6×10^{8}	3.7×10^{7}	5.6×10^{8}	8.9×10^{7}	6.0×10^{7}	6.0×10^{7}
400 K	8.3×10^{9}	2.7×10^{11}	3.6×10^{10}	6.2×10^{9}	8.2×10^{8}	6.2×10^{9}	2.0×10^{9}	1.5×10^{9}	1.5×10^{9}
500 K	4.2×10^{10}	6.8×10^{11}	1.3×10^{11}	3.3×10^{10}	6.6×10^{9}	3.3×10^{10}	1.3×10^{10}	1.0×10^{10}	1.0×10^{10}
600 K	1.3×10^{11}	1.3×10^{12}	3.4×10^{11}	1.1×10^{11}	2.7×10^{10}	1.1×10^{11}	4.8×10^{10}	4.0×10^{10}	4.0×10^{10}

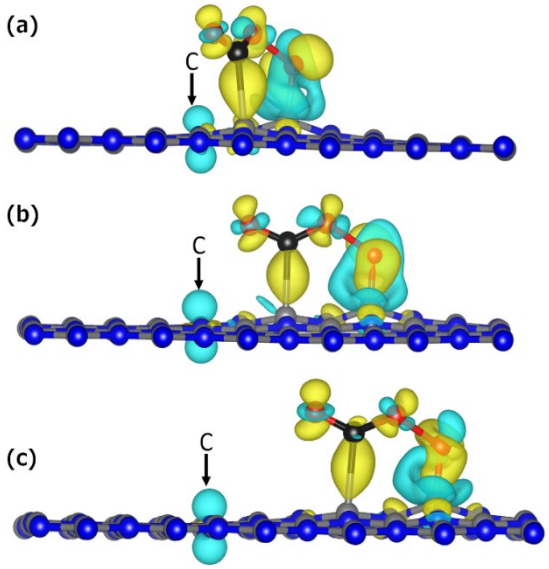

Figure 5. The electron density difference, $\rho = \rho(TS_{1\text{-}2}) - \rho(OCOO) - \rho(C_B@h\text{-}BN)$, for the co-adsorption of CO_2 molecule and O atom on C_B@h-BN surface in $TS_{1\text{-}2}$ configuration calculated for the (a) B_S, (b) B_M, and (c) B_L adsorption sites. The electron accumulation and depletion are illustrated in yellow and green, respectively. The isosurface plot is shown at +0.005 and −0.005 e/Å^3.

Figure 5 demonstrates the electron density difference, $\rho = \rho(TS_{1\text{-}2}) - \rho(OCOO) - \rho(C_B@h\text{-}BN)$, calculated for the co-adsorption of CO_2 molecule and O atom on C_B@h-BN surface in $TS_{1\text{-}2}$ at the different adsorption sites B_S, B_M, and B_L. Figure 5 shows that the electron loss from the surface mainly comes from the doped C and N atoms near the active sites. The distance between the doped C atom and the active site does not affect the electron transfer from the *p* state of the doped C atom.

C_2H_4 epoxidation reaction mechanism on the C-doped h-BN surface

Similar to the case of CO oxidation, the C_2H_4 epoxidation is also examined from the comparison of adsorption of C_2H_4 and O_2 molecules. The optimized structures and adsorption energies of O_2 and C_2H_4 adsorbed at the B_S site of C_B@h-BN are shown in Figure 2. It was shown that O_2 molecule binds much stronger than the C_2H_4 molecule, and there is no co-adsorption of O_2 and C_2H_4 on C_B@h-BN. Therefore, the O_2 adsorption is consequently the first step of the C_2H_4 epoxidation. As discussed for the CO oxidation, O_2 molecule adsorbs on top and bridge B_S sites with similar adsorption energies. In both cases the adsorbed O_2 can react with the C_2H_4 molecule along two possible pathways: (1) OC_2H_4O intermediate is formed by inserting C_2H_4 molecule into the O-O bond of the adsorbed O_2 at the bridge site, (2) OOC_2H_4 intermediate is formed by attaching C_2H_4 and the adsorbed O_2 molecule forming the bond between C and O atoms at the B sites of the surface.

Figure 6 shows the energy profile calculated for the C_2H_4 oxidation reaction along with the geometries of intermediates and transition states. As was mentioned above, the first step of the reaction is the adsorption of O_2 molecule (INT_0). After the O_2 adsorption, C_2H_4 molecule attacks the adsorbed O_2 to form the OOC_2H_4 intermediate at the top site or inserts into the O-O bond to form the OC_2H_4O intermediate. The barrier for the insertion of C_2H_4 into the O-O bond is 1.83 eV (42.2 kcal/mol), which is much higher than that of the reaction from the OOC_2H_4 intermediate (INT_2), 0.39 eV (9.0 kcal/mol). The interaction between C_2H_4 and adsorbed O_2 molecule elongates the O-O bond to accelerate the O_2 dissociation. From INT_2 O_2-C_2H_4/C_B@h-BN, the C_2H_4O and CH_3CHO formation pathways are explored based on the experimental finding that ethylene is oxidized to be either ethylene oxide or acetaldehyde intermediate [46] The activation barrier for the CH_3CHO formation pathway is calculated to be 0.96 eV (22 kcal/mol), which is higher than the

one of the C_2H_4O formation pathway. The calculated rate constant ratio of ($k_{TS2\text{-}3}$ for C_2H_4O)/($k_{TS2\text{-}3}$ for CH_3CHO) is 1.6×10^4 at 300 K. Therefore, C_2H_4O is predicted to be formed, and the residual O atom on the C_B@h-BN surface forms a stable intermediate (INT_3). The second C_2H_4 molecule then attacks the O atoms at C_B@h-BN surface to form the C_2H_4O/C_B@h-BN (INT_4 and INT'_4) with a small reaction barrier, ~0.20 eV (4.6 kcal/mol). There are also two possibilities from INT_4 and INT'_4 for the CH_3CHO and C_2H_4O formation pathways. The C_2H_4O formation is endothermic and has the activation barriers of 1.32 eV (30 kcal/mol) and 1.89 eV (44 kcal/mol) from INT_4 and INT'_4, respectively, while the CH_3CHO formation is exothermic with the lower activation barriers of 1.07 eV (25 kcal/mol) and 1.42 eV (33 kcal/mol), respectively. The calculated rate constant ratio of ($k_{TS4\text{-}5}$ for C_2H_4O)/($k_{TS4\text{-}5}$ for CH_3CHO) is 2.5×10^{-13} at 300 K. Therefore, the CH_2CH_2O formation is energetically favorable under the presence of O_2 molecule, though the CH_3CHO formation proceeds faster with O/C_B@h-BN. Note that the ratio of the yields on C_B@h-BN surface is C_2H_4O:CH_3CHO is 1:1 in one catalytic cycle.

In summary, the results of calculations suggest that the C_2H_4 epoxidation reaction on C_B@h-BN surface proceeds in the following steps:

(1) $O_2 + * \rightarrow O_2*$,

(2) $C_2H_4 + O_2* \rightarrow OOC_2H_4*$,

(3) $OOC_2H_4* \rightarrow C_2H_4O + O*$,

(4) $C_2H_4 + O* \rightarrow CH_3CHO*$.

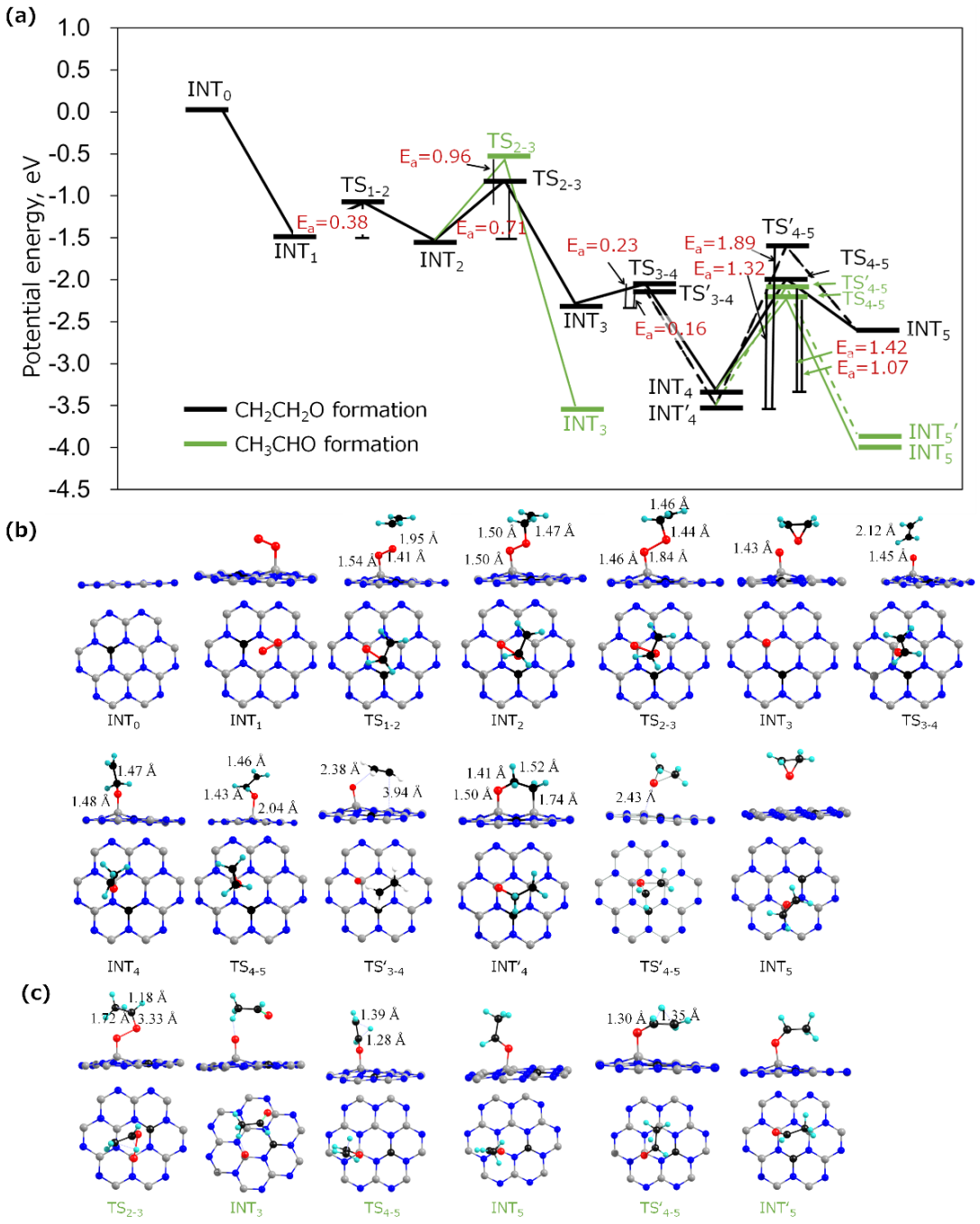

Figure 6. Energy profiles for oxidation of ethylene to ethylene oxide at B_S sites. Energies are in the unit of eV. Activation energy is written in red. The corresponding geometries are shown in (b) for CH_2CH_2O formation and (c) for CH_3CHO formation, only part of the h-BN surface is shown. The overlapped geometries are shown in (b).

Distance effect on C_2H_4 epoxidation on the C-doped h-BN surface

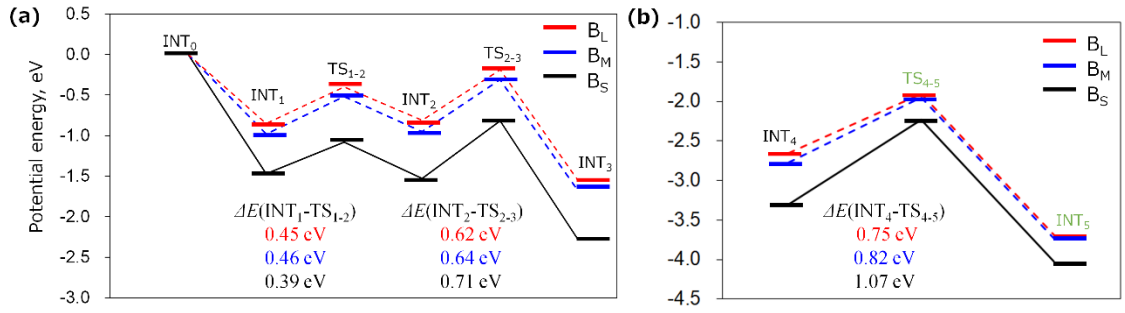

Figure 7. The distance effect on the energy profiles of C_2H_4 oxidation reaction catalyzed by C_B@h-BN. (a) reaction pathways for CH_2CH_2O formation (b) reaction pathways for CH_3CHO formation. The black, blue and red lines indicate the energy profiles for the active sites B_S, B_M, and B_L, respectively.

Finally, we investigate how the C_2H_4 epoxidation reaction proceeds on the C_B@h-BN surface at different distances from the doped C atom. **Figure 7** demonstrates the energy profiles for C_2H_4O and CH_3CHO formation calculated for the different active sites B_S, B_M, and B_L. The energy profiles show that the adsorption energies of the reaction intermediates tend to decrease relatively to INT_0 with an increase in the distance between the reaction site and the doped C atom. For C_2H_4O formation in Figure 7a, the energies for each intermediate and transition state from B_M site to B_S site increased by~ 0.55 eV, and ~0.68 eV from B_L site to B_S site.-This indicates that the energetics of the C_2H_4 epoxidation reaction on the C_B@h-BN catalyst depends on the distance from the C defect. The calculated reaction barriers for transitions from INT_1 to INT_2 via TS_{1-2} are 0.39, 0.46 and 0.45 eV for the B_S, B_M and B_L sites, respectively. This finding indicates that the values of the reaction barriers depend weakly on the distance between the reaction site and the doped C atom, at least in the considered range of distances. A similar effect is also found for the

C_2H_4 oxide formation energies from INT_2 to INT_3 via transition state $TS_{2\text{-}3}$. Thus, the activation energies for the C_2H_4 oxide formation are calculated to be 0.71, 0.64 and 0.62 eV for the B_S, B_M and B_L sites, respectively. Similar to the case of CO oxidation, the temperature effect on the rate constants is summarized in **Table 2**. The corresponding transition states are shown in Figure 7. For the CH_2CH_2O formation pathways in Figure 7(a), the predicted rate constants $k_{INT1\text{-}TS1\text{-}2}$ are evaluated as 10^5~10^6 s^{-1} in the process between INT_1 and $TS_{1\text{-}2}$ ($k_{INT1\text{-}TS1\text{-}2}$) and $10^0 \sim 10^2$ in the process between INT_2 and $TS_{2\text{-}3}$ ($k_{INT2\text{-}TS2\text{-}3}$) at 300K, indicating the low activity of the B_S, B_M and B_L sites. The rate constant at the B_S site is 16 and 10 times larger than those at B_M and B_L sites, respectively. The rate constants are increasing to $k_{INT1\text{-}TS1\text{-}2} \sim 10^9$ s^{-1} and $k_{INT2\text{-}TS2\text{-}3} \sim 10^7$ s^{-1} with the increase in temperature to 600K. This finding indicates the enhancement of the activity of these sites, significantly depending on the temperature in the CH_2CH_2O formation pathways. For the CH_3CHO formation pathways in Figure 7(b), the calculated reaction barriers from INT_4 (OC_2H_4/C_B@h-BN) are 1.07, 0.82 and 0.75 eV for the B_S, B_M and B_L sites, respectively. The calculated reaction rates increase from ~10^{-6} and ~10^0 s^{-1} at 300K to ~10^4 and ~10^6 s^{-1} at 600 K for the B_S to B_L sites, respectively. Therefore, the C_2H_4 oxidation pathway also has high temperature-dependence, though the reactivities are relatively low. This also shows that the first C_2H_4O formation is the rate-determining step of the C_2H_4 epoxidation process.

Table 2. Temperature dependence of rate constants for oxidation of C_2H_4 pathways in Figure 7.

	$k_{(INT1\text{-}TS1\text{-}2)}$, s^{-1}			$k_{(INT2\text{-}TS2\text{-}3)}$, s^{-1}			$k_{(INT4\text{-}TS4\text{-}5)}$, s^{-1}		
	B_S	B_M	B_L	B_S	B_M	B_L	B_S	B_M	B_L
300 K	1.9×10^6	1.2×10^5	1.8×10^5	7.8×10^0	1.2×10^2	2.5×10^2	7.0×10^{-6}	1.1×10^{-1}	1.7×10^0
400 K	1.1×10^8	1.4×10^7	1.9×10^7	1.0×10^4	7.6×10^4	1.4×10^5	2.9×10^{-1}	4.1×10^2	3.1×10^3
500 K	1.3×10^9	2.5×10^8	3.2×10^8	7.7×10^5	3.9×10^6	6.2×10^6	1.8×10^2	6.0×10^4	3.0×10^5
600 K	7.0×10^9	1.8×10^9	2.2×10^9	1.4×10^7	5.6×10^7	8.2×10^7	1.4×10^4	1.7×10^6	6.6×10^6

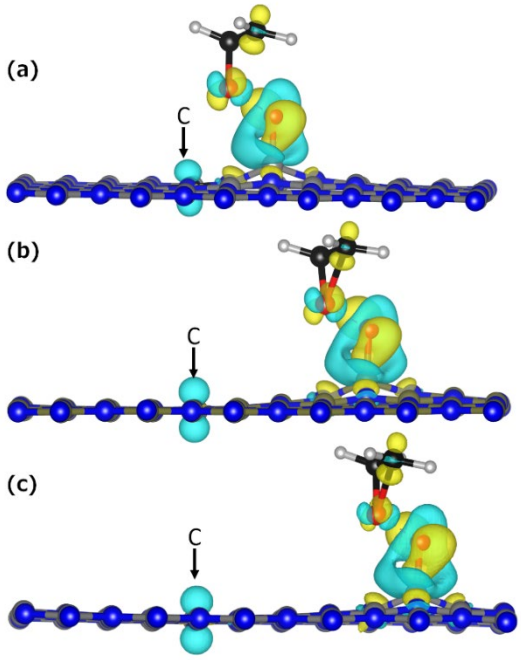

Figure 8. The distance dependence of electron density difference, $\rho = \rho(TS_{1\text{-}2}) - \rho(OOC_2H_4) - \rho(C_B@h\text{-}BN)$, for the adsorption of OOC_2H_4 intermediate on C_B@h-BN surface in $TS_{1\text{-}2}$ configuration for (a) B_S, (b) B_M, and (c) B_L sites. The electron accumulation and loss are illustrated in yellow and green, respectively. The contours are illustrated at +0.005 and −0.005 electrons per $Å^3$.

Figure 8 demonstrates the change in the electron density of the adsorbed species in $TS_{1\text{-}2}$ induced by the interaction between OOC_2H_4 intermediate and C_B@h-BN surface. As it is seen from Figure 8, the electron loss from the surface mainly comes from the doped C and N atoms near the active sites. A similar effect has been observed for the CO oxidation process. The distance between the doped C and active site does not affect the electron transfer from the *p* state of the doped C atom. Therefore, we suggest that the C-doped h-BN monolayer can be a good catalyst for

C_2H_4 epoxidation reactions due to the formation of the large catalytically active area around the C impurity.

Finally, let us consider the reliability of the calculated energy profiles. The oxidation reaction by O_2 on the h-BN surface accompanies the dissociation of O_2, in which electron transfer proceeds from the surface to O_2. However, the WC-GGA functional[29] used in the present calculations cannot quantitatively reproduce long-range electron transfers due to the neglect of long-range exchange interactions. According to the study of Janesco,[28] the long-range electron transfer from the doped C atom on the h-BN surface requires accounting for the long-range exchange effects that are included only in long-range corrected functionals. However, this study also shows that the oxidation reaction is active at distances up to ~5 Å from the doped C atom. As it was mentioned above, the B_S and B_M sites are in the activation area. This result implies that the energy profiles of the B_S and B_M sites are not so affected, though that of the B_L site, which is the most unstable and is out of the activation area, may be destabilized. We would like to note that atomically thin layer of h-BN with multiple doped C has been synthesized experimentally and proposed for the use as a potential electronic device or metal-free catalyst material.[47,48] Since the activation area is extended for the multiple C doping, C@h-BN monolayer is expected to be a promising metal-free catalyst for the oxidation reaction. It is, therefore, meaningful to systematically investigate the distance effects on the catalytic activity of C@h-BN for the oxidation reaction using O_2 molecule. This catalyst shows the way to future research on synthesizing metal-free catalysts.

IV. Conclusions

In this study, we have investigated the reactions of CO oxidation and C_2H_4 epoxidation by molecular oxygen on the C-doped hexagonal boron nitride (C_B@h-BN) monolayer catalyst. C_B@h-BN surface possesses many active sites CO oxidation and C_2H_4 epoxidation reaction as these reactions can occur at the sites located not only near but also relatively far (~ 5 Å) from the C dopant. The energy profiles of the above reactions and the dependence of the activation barriers on the distance between the doped C atom and the reaction sites are explored. As a result, we have revealed the different reaction mechanisms for the CO oxidation and C_2H_4 epoxidation reactions: CO molecule co-adsorbs and then reacts with O_2 molecule on C_B@h-BN, while C_2H_4 molecule does not adsorb on the surface and hence directly attacks the adsorbed O_2. We have also determined that the first CO_2 and C_2H_4 oxidation processes are the rate-determining steps of these reactions. Furthermore, we have found that the reaction intermediates along these reaction pathways are slightly destabilized with an increase in the distance from the doped C atom. However, the results also show that the increase in the distance between the C doped atom and the reaction sites does not affect the activation barriers strongly. Therefore, C doping of the h-BN monolayer can functionalize a large area of at least ~ 5 Å around the doped atom to be catalytically active. We, therefore, suggest that the C-doped h-BN monolayer can serve as a good catalyst for the oxidation reactions by molecular oxygen.

Corresponding Author

* Corresponding Author: gaomin@sci.hokudai.ac.jp (M. Gao), take@sci.hokudai.ac.jp (T. Taketsugu)

Notes: The authors declare no competing financial interest.

Funding Sources

Any funds used to support the research of the manuscript should be placed here (per journal style).

Notes

Any additional relevant notes should be placed here.

ACKNOWLEDGMENT

This work was financially supported by JSPS KAKENHI (17K1442907, 20K05217), the Elements Strategy Initiative of MEXT (Grant No. JPMXP0112101003), the Photo-excitonix Project at Hokkaido University, and JST CREST, Japan (Grant No. JPMJCR1902). B.W. thanks the China Scholarship Council for his PhD fellowship (CSC student number 201808050073) and the MEXT Doctoral program for Data-Related InnoVation Expert Hokkaido University (D-DRIVE-HU). The computations were performed at the Research Center for Computational Science, Okazaki, Japan.

REFERENCES

1. Fu, Q.; Bao, X., Surface chemistry and catalysis confined under two-dimensional materials. *Chem. Soc. Rev.* **2017**, *46*, 1842-1874.
2. Tan, C. L.; Cao, X. H.; Wu, X. J.; He, Q. Y.; Yang, J.;Zhang, X.; Chen, J. Z.; Zhao, W.; Han, S. K.; Nam, G. H. *et al.*, Recent Advances in Ultrathin Two-Dimensional Nanomaterials. *Chem. Rev.* **2017**, *117*, 6225-6331.
3. Cai, S. F.; Rong, H. P.; Yu, X. F.; Liu, X. W.; Wang, D. S.; He, W.; Li, Y. D., Room Temperature Activation of Oxygen by Monodispersed Metal Nanoparticles: Oxidative Dehydrogenative Coupling of Anilines for Azobenzene Syntheses. *ACS Catal.* **2013**, *3*, 478-486.
4. Montemore, M. M.; van Spronsen, M. A.; Madix, R. J.; Friend, C. M., O_2 Activation by Metal Surfaces: Implications for Bonding and Reactivity on Heterogeneous Catalysts. *Chem. Rev.* **2018**, *118*, 2816-2862.
5. Duan, X. G.; O'Donnell, K.; Sun, H. Q.; Wang, Y. X.; Wang, S. B., Sulfur and Nitrogen Co-Doped Graphene for Metal-Free Catalytic Oxidation Reactions. *Small* **2015**, *11*, 3036-3044.
6. Liu, M. Y.; Zhang, Z. R.; Liu, H. Z.; Xie, Z. B.; Mei, Q. Q.; Han, B. X., Transformation of alcohols to esters promoted by hydrogen bonds using oxygen as the oxidant under metal-free conditions. *Sci. Adv.* **2018**, *4*, eaas9319.
7. Navalon, S.; Dhakshinamoorthy, A.; Alvaro, M.; Antonietti, M.; Garcia, H., Active sites on graphene-based materials as metal-free catalysts. *Chem. Soc. Rev.* **2017**, *46*, 4501-4529.
8. Kan-Nari, N.; Okamura, S.; Fujita, S.; Ozaki, J.; Araib, M., Nitrogen-Doped Carbon Materials Prepared by Ammoxidation as Solid Base Catalysts for Knoevenagel Condensation and Transesterification Reactions. *Adv. Synth. Catal.* **2010**, *352*, 1476-1484.
9. Cao, Y. H.; Yu, H.; Peng, F.; Wang, H. J., Selective Allylic Oxidation of Cyclohexene Catalyzed by Nitrogen-Doped Carbon Nanotubes. *ACS Catal.* **2014**, *4*, 1617-1625.
10. Gao, R. J.; Pan, L.; Lu, J. H.; Xu, J. S.; Zhang, X. W.; Wang, L.; Zou, J. J., Phosphorus-Doped and Lattice-Defective Carbon as Metal-like Catalyst for the Selective Hydrogenation of Nitroarenes. *ChemCatChem* **2017**, *9*, 4287-4294.
11. Dhakshinamoorthy, A.; Primo, A.; Concepcion, P.; Alvaro, M.; Garcia, H., Doped graphene as a metal-free carbocatalyst for the selective aerobic oxidation of benzylic hydrocarbons, cyclooctane and styrene. *Chemistry* **2013**, *19*, 7547-54.
12. Lyalin, A.; Gao, M.; Taketsugu, T., When Inert Becomes Active: A Fascinating Route for Catalyst Design. *Chem. Record.* **2016**, *16*, 2324-2337.
13. Gao, M.; Lyalin, A.; Taketsugu, T., Catalytic Activity of Au and Au_2 on the h-BN Surface: Adsorption and Activation of O_2. *J. Phys. Chem. C* **2012**, *116*, 9054-9062.
14. Gao, M.; Lyalin, A.; Taketsugu, T., CO oxidation on h-BN supported Au atom. *J. Chem. Phys.* **2013**, *138*, 034701.
15. Lyalin, A.; Nakayama, A.; Uosaki, K.; Taketsugu, T., Functionalization of Monolayer h-BN by a Metal Support for the Oxygen Reduction Reaction. *J. Phys. Chem. C* **2013**, *117*, 21359-21370.
16. Lyalin, A.; Nakayama, A.; Uosaki, K.; Taketsugu, T., Adsorption and Catalytic Activation of the Molecular Oxygen on the Metal Supported h-BN. *Top. Catal.* **2014**, *57*, 1032-1041.
17. Uosaki, K.; Elumalai, G.; Noguchi, H.; Masuda, T.; Lyalin, A.; Nakayama, A.; Taketsugu, T., Boron Nitride Nanosheet on Gold as an Electrocatalyst for Oxygen Reduction Reaction: Theoretical Suggestion and Experimental Proof. *J. Am. Chem. Soc.* **2014**, *136*, 6542-6545.

18. Gao, M.; Adachi, M.; Lyalin, A.; Taketsugu, T., Long Range Functionalization of h-BN Monolayer by Carbon Doping. *J. Phys. Chem. C* **2016**, *120*, 15993-16001.
19. Uosaki, K.; Elumalai, G.; Dinh, H. C.; Lyalin, A.; Taketsugu, T.; Noguchi, H., Highly Efficient Electrochemical Hydrogen Evolution Reaction at Insulating Boron Nitride Nanosheet on Inert Gold Substrate. *Sci. Rep.* **2016**, *6*, 32217.
20. Lyalin, A.; Uosaki, K.; Taketsugu, T., Oxygen Reduction Reaction Catalyzed by Small Gold Cluster on h-BN/Au(111) Support. *Electrocatalysis* **2018**, *9*, 182-188.
21. Gao, M.; Nakahara, M.; Lyalin, A.; Taketsugu, T., Catalytic Activity of Gold Clusters Supported on the h-BN/Au(111) Surface for the Hydrogen Evolution Reaction. *J. Phys. Chem. C* **2021**, *125*, 1334-1344.
22. Grant, J. T.; Carrero, C. A.; Goeltl, F.;Venegas, J.; Mueller, P.; Burt, S. P.; Specht, S. E.; McDermott, W. P.; Chieregato, A.; Hermans, I., Selective oxidative dehydrogenation of propane to propene using boron nitride catalysts. *Science* **2016**, *354*, 1570-1573.
23. Han, R.; Diao, J. Y.; Kumar, S.; Lyalin, A.; Taketsugu, T.; Casillas, G.; Richardson, C.; Liu, F.; Yoon, C. W.; Liu, H. Y.; Sun, X. D.; Huang, Z. G., Boron nitride for enhanced oxidative dehydrogenation of ethylbenzene. *J. Energy. Chem.* **2021**, *57*, 477-484.
24. Lyalin, A.; Uosaki, K.; Taketsugu, T., Oxygen Reduction Reaction Catalyzed by Small Gold Cluster on h-BN/Au(111) Support. *Electrocatalysis* **2017**, *9*, 182-188.
25. Shao, M.; Chang, Q.; Dodelet, J. P.; Chenitz, R., Recent Advances in Electrocatalysts for Oxygen Reduction Reaction. *Chem. Rev.* **2016**, *116*, 3594-657.
26. Markovic, N. M.; Schmidt, T. J.; Stamenkovic, V.; Ross, P. N., Oxygen Reduction Reaction on Pt and Pt Bimetallic Surfaces: A Selective Review. *Fuel Cells* **2001**, *1*, 105-116.
27. Gao, M.; Adachi, M.; Lyalin, A.; Taketsugu, T., Long Range Functionalization of h-BN Monolayer by Carbon Doping. *J. Phys. Chem. C* **2016**, *120*, 15993-16001.
28. Janesko, B. G., Delocalization Error in DFT-Predicted Extreme Long-Range Functionalization of Carbon-Doped Hexagonal Boron Nitride. *J. Phys. Chem. C* **2019**, *123*, 15062-15070.
29. Wu, Z. G.; Cohen, R. E., More accurate generalized gradient approximation for solids. *Phy.Rev. B* **2006**, *73*, 235116.
30. Giannozzi, P.; Baroni, S.; Bonini, N.; Calandra, M.; Car, R.; Cavazzoni, C.; Ceresoli, D.; Chiarotti, G. L.; Cococcioni, M.; Dabo, I. Dal Corso, A.; de Gironcoli, S.; Fabris, S.; Fratesi, G.; Gebauer, R.; Gerstmann, U.; Gougoussis, C.; Kokalj, A.; Lazzeri, M.; Martin-Samos, L.; Marzari, N.;Mauri, F.; Mazzarello, R.; Paolini, S.; Pasquarello, A.; Paulatto, L.; Sbraccia, C.; Scandolo, S.; Sclauzero, G.; Seitsonen, A. P.;Smogunov, A.; Umari, P.; Wentzcovitch, R. M., QUANTUM ESPRESSO: a modular and open-source software project for quantum simulations of materials. *J. Phys-Condens Mat.* **2009**, *21*, 395502.
31. Yoo, C. S.; Akella, J.; Cynn, H.; Nicol, M., Direct elementary reactions of boron and nitrogen at high pressures and temperatures. *Phy. Rev. B* **1997**, *56*, 140-146.
32. Henkelman, G.; Uberuaga, B. P.; Jonsson, H., A climbing image nudged elastic band method for finding saddle points and minimum energy paths. *J. Chem. Phys.* **2000**, *113*, 9901-9904.
33. Henkelman, G.; Arnaldsson, A.; Jonsson, H., A fast and robust algorithm for Bader decomposition of charge density. *Comp. Mats.Sci.* **2006**, *36*, 354-360.
34. Momma, K.; Izumi, F., VESTA: a three-dimensional visualization system for electronic and structural analysis. *J. Appl. Crystallogr.* **2008**, *41*, 653-658.

35. Haruta, M.; Kobayashi, T.; Sano, H.; Yamada, N., Novel Gold Catalysts for the Oxidation of Carbon-Monoxide at a Temperature Far Below 0 C. *Chem. Lett.* **1987**, 405-408.
36. Haruta, M., Size- and support-dependency in the catalysis of gold. *Catal. Today* **1997**, *36*, 153-166.
37. Landman, U.; Yoon, B.; Zhang, C.; Heiz, U.; Arenz, M., Factors in gold nanocatalysis: oxidation of CO in the non-scalable size regime. *Top Catal.* **2007**, *44*, 145-158.
38. Yoon, B.; Hakkinen, H.; Landman, U.; Worz, A. S.; Antonietti, J. M.; Abbet, S.; Judai, K.; Heiz, U., Charging effects on bonding and catalyzed oxidation of CO on Au-8 clusters on MgO. *Science* **2005**, *307*, 403-407.
39. Sanchez, A. Abbet, S.; Heiz, U.; Schneider, W. D.; Häkkinen, H.; Barnett, R. N.; Landman, U., When Gold Is Not Noble: Nanoscale Gold Catalysts. *J. Phys. Chem. A* **1999**, *103*, 9573-9578.
40. Haruta, M.; Date, M., Advances in the catalysis of Au nanoparticles. *Appl. Catal. A-Gen.* **2001**, *222*, 427-437.
41. Kung, H. H.; Kung, M. C.; Costello, C. K., Supported Au catalysts for low temperature CO oxidation. *J. Catal.* **2003**, *216*, 425-432.
42. Socaciu, L. D.; Hagen, J.; Bernhardt, T. M.; Woste, L.; Heiz, U.; Hakkinen, H.; Landman, U., Catalytic CO oxidation by free Au_2: Experiment and theory. *J. Am. Chem. Soc.* **2003**, *125*, 10437-10445.
43. Soares, J. M. C.; Bowker, M., Low temperature CO oxidation on supported and unsupported gold compounds. *Appl. Catal. A-Gen.* **2005**, *291*, 136-144.
44. Lu, Z.; Lv, P.; Xue, J.; Wang, H.; Wang, Y.; Huang, Y.; He, C.; Ma, D.; Yang, Z., Pd_1/BN as a promising single atom catalyst of CO oxidation: a dispersion-corrected density functional theory study. *RSC Adv.* **2015**, *5*, 84381-84388.
45. Dumesic J. A.; Rudd D. F.; Aparicio L. M.; Rekoske J. E.; Treviño A. A., The Microkinetics of Heterogeneous Catalysis, American Chemical Society, Washington DC, 1993.
46. Pu, C.; Tian, H.; Ford, M. E. F.; Rangarajan S.; Wachs I. E. *ACS Catal*. **2019**, 9, 10727-10750.
47. Ci, L.; Song, L.; Jin, C.; Jariwala, D.; Wu, D.; Li, Y.; Srivastava, A.; Wang, Z. F.; Storr, K.; Balicas, L.; Liu, F.; Ajayan, P. M., Atomic layers of hybridized boron nitride and graphene domains. *Nat. Mater.* **2010**, *9*, 430-5.
48. Zhang, K. X.; Su, H.; Wang, H. H.; Zhang, J. J.; Zhao, S. Y.; Lei, W.; Wei, X.; Li, X. H.; Chen, J. S., Atomic-Scale Mott-Schottky Heterojunctions of Boron Nitride Monolayer and Graphene as Metal-Free Photocatalysts for Artificial Photosynthesis. *Adv. Sci.* **2018**, *5*, 1800062.